Comparison between high-frequency irreversible electroporation and irreversible electroporation ablation of small swine liver: follow-up of DCE-MRI and pathological observations

Jing Li[1,2], Xiao-Bo Zhang[3], Jing-Jing Wang[4], Lu-Jia Jin[5], Hu-Sheng Shan[3,6], Xiao Zhang[3], Li Ma[7], Xiao-Dong Xue[3], Xin Zhang[3], Zhong-Liang Zhang[3], Liang-Liang Meng[3], Fei Yuan[2], Yue-Yong Xiao[3]

[1]Medical School of Chinese People's Liberation Army, Beijing 100853, China;
[2]Department of Radiology, Characteristic Medical Center of Chinese People's Armed Police Force, Tianjin 300162, China;
[3]Department of Radiology, The First Medical Center of the General Hospital of the People's Liberation Army, Beijing 100853, China;
[4]Department of Intensive Care Unit, Tianjin First Central Hospital, Tianjin 300152, China;
[5]Department of General Surgery, The First Medical Center of the General Hospital of the People's Liberation Army, Beijing 100853, China;
[6]Department of Radiotherapy, Huai'an Medical Area, General Hospital of the Eastern Theater Command, Huai'an, Jiangsu 223001, China;
[7]Department of Anesthesiology, The First Medical Center of the General Hospital of the People's Liberation Army, Beijing 100853, China.

Abstract

Background: High-frequency irreversible electroporation (H-FIRE) is a novel, next-generation nanoknife technology with the advantage of relieving irreversible electroporation (IRE)-induced muscle contractions. However, the difference between IRE and H-FIRE with distinct ablation parameters was not clearly defined. This study aimed to compare the efficacy of the two treatments *in vivo*.

Methods: Ten Bama miniature swine were divided into two group: five in the 1-day group and five in the 7-day group. The efficacy of IRE and H-FIRE ablation was compared by volume transfer constant (Krans), rate constant (Kep) and extravascular extracellular volume fraction (Ve) value of dynamic contrast-enhanced magnetic resonance imaging (DCE-MRI), size of the ablation zone, and histologic analysis. Each animal underwent the IRE and H-FIRE. Temperatures of the electrodes were measured during ablation. DCE-MRI images were obtained 1, 4, and 7 days after ablation in the 7-day group. All animals in the two groups were euthanized 1 day or 7 days after ablation, and subsequently, IRE and H-FIRE treated liver tissues were collected for histological examination. Student's *t* test or Mann-Whitney *U* test was applied for comparing any two groups. One-way analysis of variance (ANOVA) test and Welch's ANOVA test followed by Holm-Sidak's multiple comparisons test, one-way ANOVA with repeated measures followed by Bonferroni test, or Kruskal-Wallis *H* test followed by Dunn's multiple comparison test was used for multiple group comparisons and *post hoc* analyses. Pearson correlation coefficient test was conducted to analyze the relationship between two variables.

Results: Higher Ve was seen in IRE zone than in H-FIRE zone (0.14 ± 0.02 *vs.* 0.08 ± 0.05, $t = 2.408$, $P = 0.043$) on day 4, but no significant difference was seen in Ktrans or Kep between IRE and H-FIRE zones at all time points (all $P > 0.05$). For IRE zone, the greatest Ktrans was seen on day 7, which was significantly higher than that on day 1 ($P = 0.033$). The ablation zone size of H-FIRE was significantly larger than IRE 1 day (4.74 ± 0.88 cm^2 *vs.* 3.20 ± 0.77 cm^2, $t = 3.241$, $P = 0.009$) and 4 days (2.22 ± 0.83 cm^2 *vs.* 1.30 ± 0.50 cm^2, $t = 2.343$, $P = 0.041$) after treatment. Apoptotic index (0.05 ± 0.02 *vs.* 0.73 ± 0.06 *vs.* 0.68 ± 0.07, $F = 241.300$, $P < 0.001$) and heat shock protein 70 (HSP70) (0.03 ± 0.01 *vs.* 0.46 ± 0.09 *vs.* and 0.42 ± 0.07, $F = 64.490$, $P < 0.001$) were significantly different between the untreated, IRE and H-FIRE zones, but no significant difference was seen in apoptotic index or HSP70 between IRE and H-FIRE zone (both $P > 0.05$). Electrode temperature variations were not significantly different between the two zones (18.00 ± 3.77°C *vs.* 16.20 ± 7.45°C, $t = 0.682$, $P = 0.504$). The Ktrans value ($r = 0.940$, $P = 0.017$) and the Kep value ($r = 0.895$, $P = 0.040$) of the H-FIRE zone were positively correlated with the number of hepatocytes in the ablation zone.

Conclusions: H-FIRE showed a comparable ablation effect to IRE. DCE-MRI has the potential to monitor the changes of H-FIRE ablation zone.

Keywords: Irreversible electroporation; High-frequency irreversible electroporation; Dynamic contrast enhanced-magnetic resonance imaging; Thermal damage

Access this article online

Quick Response Code:

Website: www.cmj.org

DOI: 10.1097/CM9.0000000000001663

Jing Li, Xiao-Bo Zhang, and Jing-Jing Wang contributed equally to this work.

Correspondence to: Dr. Yue-Yong Xiao, Department of Radiology, The First Medical Center of the General Hospital of the People's Liberation Army, Beijing 100853, China
E-Mail: xyy301radiology@gmail.com

Chinese Medical Journal 2021;134(17)
Received: 29-03-2021 **Edited by:** Pei-Fang Wei

Introduction

Irreversible electroporation (IRE), also known as nanoknife ablation, is a novel technology of non-thermal ablation, which utilizes high-voltage electrical pulses to induce nanometer-scale pores in the cell membrane, leading to cell death and tissue necrosis. Its non-thermal effect allows for IRE application in the porta hepatis and pancreas, since IRE promotes sparing of sensitive structures, including blood vessel, bile ducts, pancreatic duct, and nerve architecture.[1] However, several issues limit the IRE application in clinical practice.[2,3] Severe muscle contractions induced by electrical impulse can affect the safety and efficacy of surgery, and the use of paralytic agents is needed to control convulsions.[4] Therefore, general anesthesia is required for patients receiving IRE therapy because mechanical ventilation is necessary to avoid hypoxia and asphyxia due to respiratory inhibition after the use of paralytic agents.

To overcome these disadvantages, high-frequency irreversible electroporation (H-FIRE), a novel, next-generation nanoknife technology, was developed. H-FIRE utilizes high-frequency bipolar bursts to minimize muscle contraction, in which the effect of the first pulse was canceled by the effect of the second pulse of the opposite polarity. The pulse duration and the inter-phase delay are the main factors influencing the cancellation effect, and shorter pulses and shorter interphase delay cause more pronounced cancellation.[5] H-FIRE obviates the need for paralytic agents and eliminates the inherent risk associated with general anesthesia, in doing so, optimizes the surgical procedure and makes the surgery less complicated to provide the possibility for performance in more patients.[6] The different waveforms and frequencies of IRE and H-FIRE affect the cell death and repair in distinct ways.[7] However, little is known regarding the difference of effects and mechanisms between IRE and H-FIRE *in vivo*, and the efficacy of H-FIRE treatment *in vivo* is also not clearly determined.

Magnetic resonance imaging (MRI) is considered to be ideal for the assessment of IRE response in liver tissues.[8] Dynamic contrast-enhanced MRI (DCE-MRI) can be particularly effective for visualization of tissue perfusion, vascular blood flow, blood vessel permeability, and tissue contrast uptake. Furthermore, the extravascular extracellular volume fraction (Ve) can be calculated from DCE-MRI by quantitative MRI measurements such as volume transfer constant (Ktrans) and rate constant (Kep). Previous publications also showed that DCE-MRI can be used to distinguish between IRE and reversible electroporation (RE) zones of IRE treatment.[9] Nevertheless, limited studies implemented DCE-MRI for assessment of H-FIRE treatment, or compared the post-treatment quantitative MRI changes between IRE and H-FIRE. Therefore, more insight into the DCE-MRI of IRE and H-FIRE is needed in order to guide the application in clinical practice.

We aimed to investigate the efficacy of H-FIRE in the porcine liver by comparing the temperature, size of the ablation zone, changes of DCE-MRI, histologic analysis, and transmission electron microscope appearance between H-FIRE and IRE.

Methods

Ethical approval

All experiments were approved by the Institutional Animal Ethics Committee of the General Hospital of the People's Liberation Army (No. 2019-D15–23) and performed in accordance with the international ethics for animal use.

Animal model

Ten Bama miniature swine (Shi-Chuang Animal Labs, Beijing, China) underwent IRE and H-FIRE as well as baseline and postprocedural MRI. Injection of midazolam (0.5 mg/kg) and xylazine hydrochloride (20 mg/kg) were given to induce anesthesia. Ventilation with isoflurane (2.5% with 100% oxygen, 3 L/min, Patterson Veterinary, Greeley, CO, USA) via breathing mask was used for anesthesia maintenance throughout imaging and IRE/H-FIRE procedure. Five animals were euthanized one day after surgery, and five animals were euthanized seven days after procedure. Swine were euthanized by intravenous injection of euthanasia solutions containing pentobarbital sodium (200 mg/kg).

Overview of experimental design

This experiment was performed in porcine livers. The flow diagram of the study design is summarized in Figure 1. Animals were divided into a 1-day group and a 7-day group. Each animal underwent the IRE and H-FIRE procedure at two sites with a distance of over 6 cm in the liver which is longer than that reported in previous literature.[10] The temperature of the electrode was measured and collected during ablation in the 1-day group. DCE-MRI images were obtained 1, 4, and 7 days after the procedure in the 7-day group. Both treated and untreated liver tissues were collected for histology in the 1-day group, and only treated liver tissues were collected for histological examination in the 7-day group. Animals in the 1-day group were euthanized one day after surgery, and those in the 7-day group were euthanized seven days after surgery.

IRE and H-FIRE ablation

The liver was exposed by laparotomy. Two paralleled needle electrodes with 1.5 cm spacing (platinum-iridium materials; Microprobes, Inteligent Health, Tianjin) were inserted into the liver with a 1.5 cm depth. Electrode separation was maintained by securing the needles in a plastic spacing block. Next, the electrodes were connected to the IRE generator (YTL-GM01, Inteligent Health) to apply 2200 V square wave pulses (number of pulses, 100; each pulse duration, 100 μs; interval between pulses, 1000 ms; Supplementary Figure 1, http://links.lww.com/CM9/A703). H-FIRE therapy was delivered through a custom-built H-FIRE waveform generator (Inteligent Health). The generator was set to deliver 3000 V asymmetric square wave pulses (number of pulses, 2400). Within an individual burst of bipolar pulses, a 5 μs positive pulse, 3 μs inter-pulse delay, 3 μs negative pulse, and a 5 μs inter-pulse delay pattern was repeated [Supplementary Figure 1, http://links.lww.com/CM9/A703]. Two authors (JL and XBZ, both with at least 4-year experience) performed IRE and H-FIRE ablation procedures for about 10 minutes.

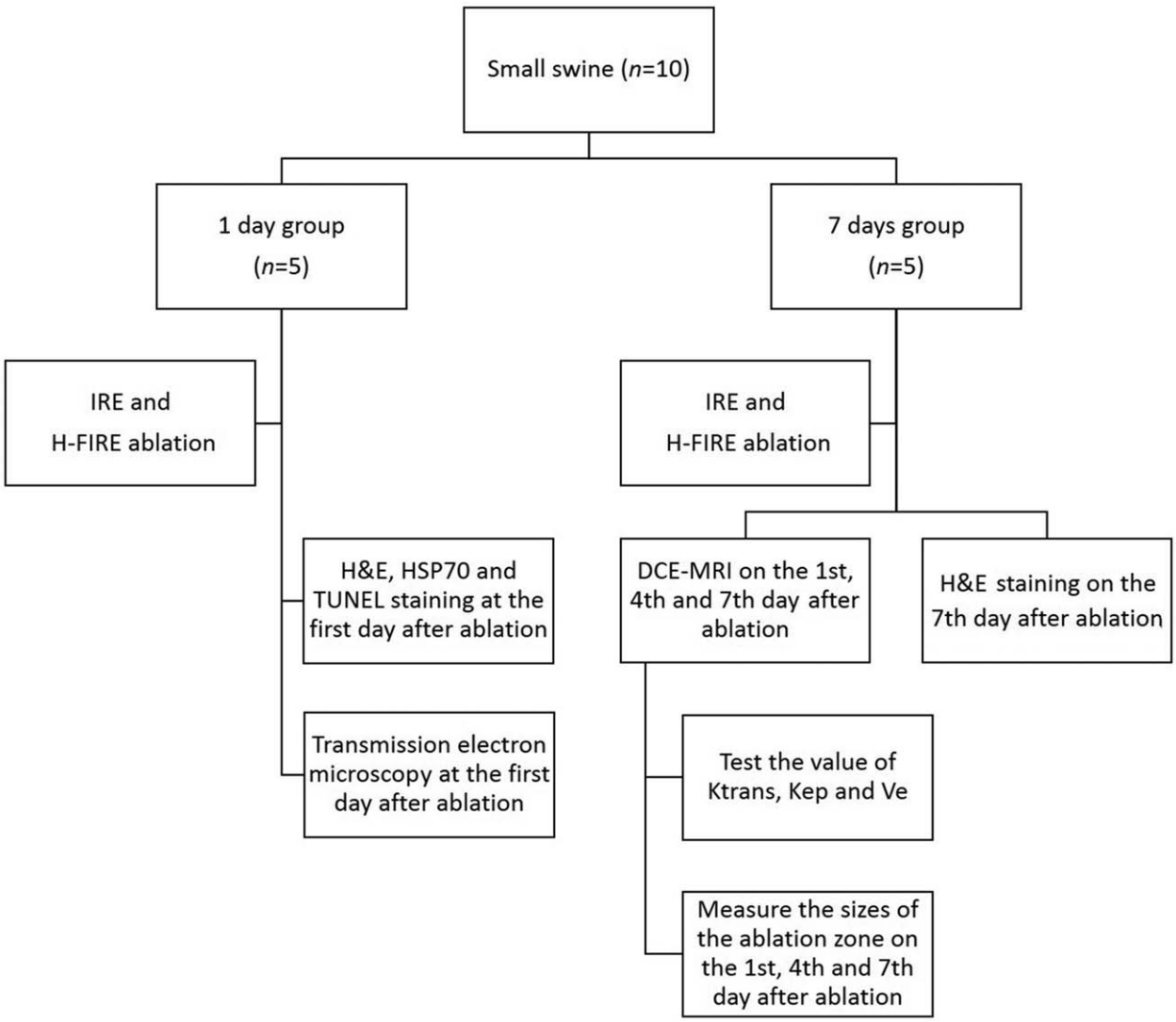

Figure 1: Flow diagram for comparison between H-FIRE and IRE ablation in small swine liver. DCE-MRI: Dynamic contrast-enhanced magnetic resonance imaging; H&E: Haematoxylin and eosin; H-FIRE: High-frequency irreversible electroporation; HSP70: Heat shock protein 70; IRE: Irreversible electroporation; Kep: Rate constant; Ktrans: Volume transfer constant; TUNEL: Terminal deoxynucleotidyl transferase-mediated deoxyuridine triphosphate nick end labeling; Ve: Extravascular extracellular volume fraction.

DCE-MRI examination

All images were acquired using an abdominal coil (32-Channel abdominal Coil; General Electric [GE], Fairfield, CT, USA) in a 3.0 T clinical MRI unit (GE, MAGNETOM 750W 3.0 T), with the animal in a prone position. Five animals in the 7-day group underwent MRI imaging on days 1, 4, and 7. DCE-MRI was performed using a liver acquisition with volume acceleration (LAVA) sequence which consisted of Echo 1/1, time of echo (TE) 1.7 ms, time of inversion (TI) 7.0 ms, thickness 4.0 mm, the field of view (FOV) 240 mm× 240 mm, matrix 256 × 160, and number of excitations (NEX) 0.71. A total of 1200 images of the targeted sections covering 40 phases were acquired every 2.6 s. During image acquisition, baseline DCE-MRI images were acquired for 60 s. After initial image acquisition, 0.1 mmol/kg gadobenate dimeglumine (Gd-BOPTA) solution (MultiHance; Bracco Sine, Shanghai, China) was delivered at 2 mL/s via an ear-vein catheter, followed by flushing with 10 mL saline through the same ear-vein catheter.

DCE-MRI analysis

All DCE-MRI images were initially post-processed using AW4.6 (GE). Region of interests (ROIs) were drawn around the ablation zones of IRE and H-FIRE treatment with anatomic T2 fat saturation (T2FS) and single-shot fast spin echo (SSFSE) images as reference. ROI was confined to the ablation zone without exceeding the edge of the ablation zone, and vessels should be excluded from the ROI. Quantitative measurements of DCE-MRI were conducted using AW4.6 post-processing workstation. A dual-inlet two-compartment modified Tofts model was used to calculate the following quantitative measurements: Ktrans, Kep, and Ve.

Measurement of the ablation zone

The size of the irreversible ablation zone was assessed and measured using DCE-MRI at the sixth phase one day after IRE and H-FIRE treatment at the largest level of the

ablation zone. Similar to prior studies,[9,11] the irreversible ablation zone size was defined as the unenhanced region on contrast-enhanced MRI with reduced signal intensity as compared with untreated liver tissue.

Transmission electron microscope observation

Specimens with a size of 3 mm^3 were obtained from the ablation zone center of IRE and H-FIRE treatment, as well as untreated liver tissue in one animal. Tissues were fixed in glutaraldehyde, and post-fixed in 1% osmium tetroxide. Tissue dehydration was performed with serial concentrations of ethanol, and embedded in Epon. Then specimens were sliced into 750-nm thickness. The samples were stained with 2% uranyl acetate and lead citrate for 15 minutes each. They were then examined using a transmission electron microscope to collect images.

Histologic analysis

IRE-treated, H-FIRE treated, and fresh untreated livers were fixed in formalin, and sliced for hematoxylin and eosin (H&E) staining, heat shock protein 70 (HSP70) staining, and terminal deoxynucleotidyl transferase-mediated deoxyuridine triphosphate nick-end labeling (TUNEL) assays. Images of pathology were digitally analyzed by ImageJ (NIH, USA). Apoptotic index was calculated as the percentage of apoptotic cells through reading the cells in five selected fields at a 400-fold magnification microscopy. In the IRE and H-FIRE ablation zone of the 7-day group, 5 high-powered fields with 1000 × magnification were randomly selected for hepatic cell counting.

Temperature monitoring

In order to avoid the influence of the strong electric field on the thermistor to obtain the actual temperature change during the ablation of the IRE and H-FIRE, we measured the temperature by laser through placement of a Bragg grating in the electrode [Supplementary Figure 2A and 2B, http://links.lww.com/CM9/A703]. Since the effect on the wavelength change is primarily due to the change in the refractive index of the silicon dioxide caused by the thermo-optic effect, once the time shift of the wavelength in the ablation is measured, the temperature variation during each ablation is obtained by converting the strain dependence of Bragg grating.[12]

Statistical analysis

All statistical analyses were conducted using GraphPad Prism (GraphPad Software, La Jolla, CA, USA). Shapiro-wilk test and Q-Q plot were used to analyze the normality of the continuous variables. Continuous variables with normal distribution were presented as mean ± standard deviation, and those with non-normal distribution were shown as median (Q_1, Q_3). Student's *t* test or Mann-Whitney *U* test was applied for comparing any two groups. One-way analysis of variance (ANOVA) test and Welch's ANOVA test followed by Holm-Sidak's multiple comparisons test, one-way ANOVA with repeated measures followed by Bonferroni test, or Kruskal-Wallis *H* test followed by Dunn's multiple comparison test was used for multiple group comparisons and *post hoc* analyses. $P < 0.017$ was considered statistically significant for Bonferroni *post hoc* analyses. $P < 0.05$ was considered statistically significant for the other tests and *post hoc* analyses. Pearson correlation coefficient test was conducted to analyze the relationship between two variables.

Results

Tip temperature variations of IRE and H-FIRE were similar

The temperature was measured by Bragg grating in the electrode during ablation. The temperature variation was 18.00 ± 3.77°C and 16.20 ± 7.45°C for IRE and H-FIRE, respectively, without a statistically significant difference ($t = 0.682$, $P = 0.504$) [Supplementary Figure 2C, http://links.lww.com/CM9/A703].

Similar DCE-MRI findings were seen in IRE-and H-FIRE ablation zone

Table 1 calculated and summarized parameters of IRE zone and H-FIRE zone on days 1, 4, and 7 after ablation. No significant differences were detected in Ktrans, Kep, or

Table 1: Comparison of Ktrans, Kep and Ve between IRE and H-FIRE zones.

Items	IRE ($n = 5$)	H-FIRE ($n = 5$)	Statistics	*P*
Day 1				
Ktrans (/min)	0.07 ± 0.03	0.08 ± 0.05	0.432*	0.677
Kep (/min)	0.61 ± 0.30	0.56 ± 0.15	0.344*	0.740
Ve	0.09 (0.06, 0.29)	0.12 (0.06, 0.30)	12.000†	0.999
Day 4				
Ktrans (/min)	0.12 (0.06, 0.45)	0.08 (0.06, 0.09)	7.000†	0.310
Kep (/min)	0.84 ± 0.36	0.90 ± 0.34	0.291*	0.778
Ve	0.14 ± 0.02	0.08 ± 0.05	2.408*	0.043
Day 7				
Ktrans (/min)	0.17 ± 0.07	0.18 ± 0.06	0.317*	0.759
Kep (/min)	0.64 ± 0.33	0.92 ± 0.59	0.895*	0.397
Ve	0.21 ± 0.11	0.20 ± 0.08	0.228*	0.825

Data are presented as mean ± standard deviation or median (Q_1, Q_3). *t values. †U values. H-FIRE: High-frequency irreversible electroporation; IRE: Irreversible electroporation; Kep: Rate constant; Ktrans: Volume transfer constant; Ve: Extravascular extracellular volume fraction.

Ve between IRE zone and H-FIRE zone on day 1 and day 7 (all $P > 0.05$). A significantly higher Ve was seen in the IRE zone than H-FIRE zone on day 4 (0.14 ± 0.02 *vs.* 0.08 ± 0.05, $t = 2.408$, $P = 0.043$), while no significant difference was seen in Ktrans or Kep between IRE zone and H-FIRE zone (both $P > 0.05$).

For H-FIRE zone, we did not observe significant differences in Ktrans, Kep, or Ve of the ablation zone, respectively, between day 1, day 4, and day 7 (all $P > 0.05$). For IRE zone, the greatest Ktrans was seen on day 7, which was significantly higher than that on day 1 ($P = 0.033$); no significant difference in Kep or Ve was recorded over time (both $P > 0.05$) [Table 1, Figure 2].

H-FIRE ablation zone was larger than that of IRE

Ablation zone sizes are shown in Table 2. Figure 3 gives a graphical overview of the progression of the ablation zone sizes measured 1, 4, and 7 days after treatment. Significant decrease of ablation zone size was seen over time in IRE zone ($3.20 \pm 0.77\ cm^2$ *vs.* $1.30 \pm 0.50\ cm^2$ *vs.* $0.73 \pm 0.26\ cm^2$, $W = 26.610$, $P < 0.001$) and H-FIRE zone ($4.74 \pm 0.88\ cm^2$ *vs.* $2.22 \pm 0.83\ cm^2$ *vs.* $1.30 \pm 0.68\ cm^2$, $W = 27.480$, $P < 0.001$), respectively. H-FIRE had larger ablation zone sizes than IRE 1 day ($4.74 \pm 0.88\ cm^2$ *vs.* $3.20 \pm 0.77\ cm^2$, $t = 3.241$, $P = 0.009$) and 4 days after treatment ($2.22 \pm 0.83\ cm^2$ *vs.* $1.30 \pm 0.50\ cm^2$, $t = 2.343$, $P = 0.041$).

IRE showed similar ablation effect to H-FIRE on the basis of electron microscopy, gross pathology, and histologic changes

After IRE or H-FIRE treatment, the hepatocytes showed lysis of the plasma membrane with cytoplasm swelling and intracellular vacuoles on electron microscopy. Karyopyknosis and condensed chromatin in margin were observed. Mitochondria appeared irregular with slight swelling, broken membrane, as well as fracture, reduction, and loss of cristae. We also found some lipid droplets, secondary lysosomes and autophagosomes in the cells [Supplementary Figure 3A–C, http://links.lww.com/CM9/A703].

Figure 4 showed representative gross pathology and histology of IRE zone, H-FIRE zone, and untreated tissues for HSP70, TUNEL, and H&E staining. One day after surgery, clear demarcation (or margin) between IRE zone/H-FIRE zone and untreated tissues was seen in the gross specimen [Figure 4A]. Following H&E, HSP70 [Figure 4B], and TUNEL staining [Figure 4C], the IRE and H-FIRE zones showed large areas of red discoloration and hemorrhagic infiltration. The liver tissue failed to retain its structure with extensive necrosis in the area with overexpression of HSP70 and cell apoptosis. The apoptotic index was 0.05 ± 0.02, 0.73 ± 0.06 and 0.68 ± 0.07 for the untreated tissue, IRE zone, and H-FIRE zone, respectively ($F = 241.300$, $P < 0.001$). IRE ($P < 0.001$) zone and H-FIRE ($P < 0.001$) zone had a significantly higher apoptotic index as compared with untreated tissue, while no significant difference was detected between IRE zone and H-FIRE zone ($P = 0.450$). There was significant differences among the untreated, IRE and H-FIRE zone in the percentage of HSP70-positive cells ($F = 64.490$, $P < 0.001$). The percentage of HSP70-positive cells increased after IRE and H-FIRE treatment compared with the untreated tissue (0.46 ± 0.09 *vs.* 0.03 ± 0.01, $P < 0.001$; 0.42 ± 0.07 *vs.* 0.03 ± 0.01, $P < 0.001$, respectively), while no significant difference was detected between IRE zone and H-FIRE zone ($P = 0.604$). After 7 days, the gross pathology [Figure 5A] and H&E staining [Figure 5B] revealed significantly shrinking IRE zone and H-FIRE zone with fibrosis. The lobular architecture was not conserved with margin infiltrated by the inflammatory cells. No extensive necrosis or hemorrhage was observed in the ablation zone. White coagulation necrosis and fibrosis were visible along the electrode tracks of IRE, and vessels and bile ducts remained intact.

DCE-MRI can reflect the pathophysiological changes of H-FIRE zone

DCE-MRI reveals the distribution of contrast agent between the blood vessel and the extracellular space, which indirectly reflects the metabolism in the tissue. Figure 6 showed the comparison of the correlation between the number of hepatocytes in the IRE and H-FIRE ablation zone with Kep, Ktrans, and Ve. The Ktrans value ($r = 0.940$, $P = 0.017$) and the Kep value ($r = 0.895$, $P = 0.040$) of the H-FIRE zone were positively correlated with the number of hepatocytes in the ablation zone. However, the Ve value of the H-FIRE zone and the Kep, Ktrans, Ve values of the IRE zone showed no correlation with the number of hepatocytes ($P > 0.05$).

Discussion

Emerging evidence showed the potential of H-EIRE in the treatment of malignant neoplasms.[5-7,11,13] However, its efficacy and safety have not yet been thoroughly evaluated since most studies were conducted with usage of *ex vivo* swine model, and lacked dynamic comparison with conventional IRE treatment.[7,14-16]

DCE-MRI is a functional imaging technique with continuous, repeated, and rapid imaging. It provides superior information about the tissues' physiological properties on the basis of the microvascular system in tissues and lesions. Semi-quantitative or quantitative parameters can be derived from calculation and analysis of the images obtained before and after injection of contrast agent into the bloodstream.[17] Owing to the advantages of quantitative analysis over semi-quantitative analysis, a dual-input two-compartment pharmacokinetic model (a dual-input extended Tofts model and a dual-input 2-compartment exchange model) was implemented in the current study to calculate the Ktrans, Kep, and Ve.[18,19] Kep = Ktrans/Ve was set in the two-compartment pharmacokinetic model. Ktrans is an important pharmacokinetic parameter to assess infiltration surface area per unit volume of tissue. The distribution of contrast agents is influenced by the cooperation of vascular permeability and plasma flow, therefore, Ktrans is determined by these two factors. A higher Ktrans value is associated with increased vascular permeability and plasma flow of tissue. DCE-MRI is considered an effective tool to reflect the capillary

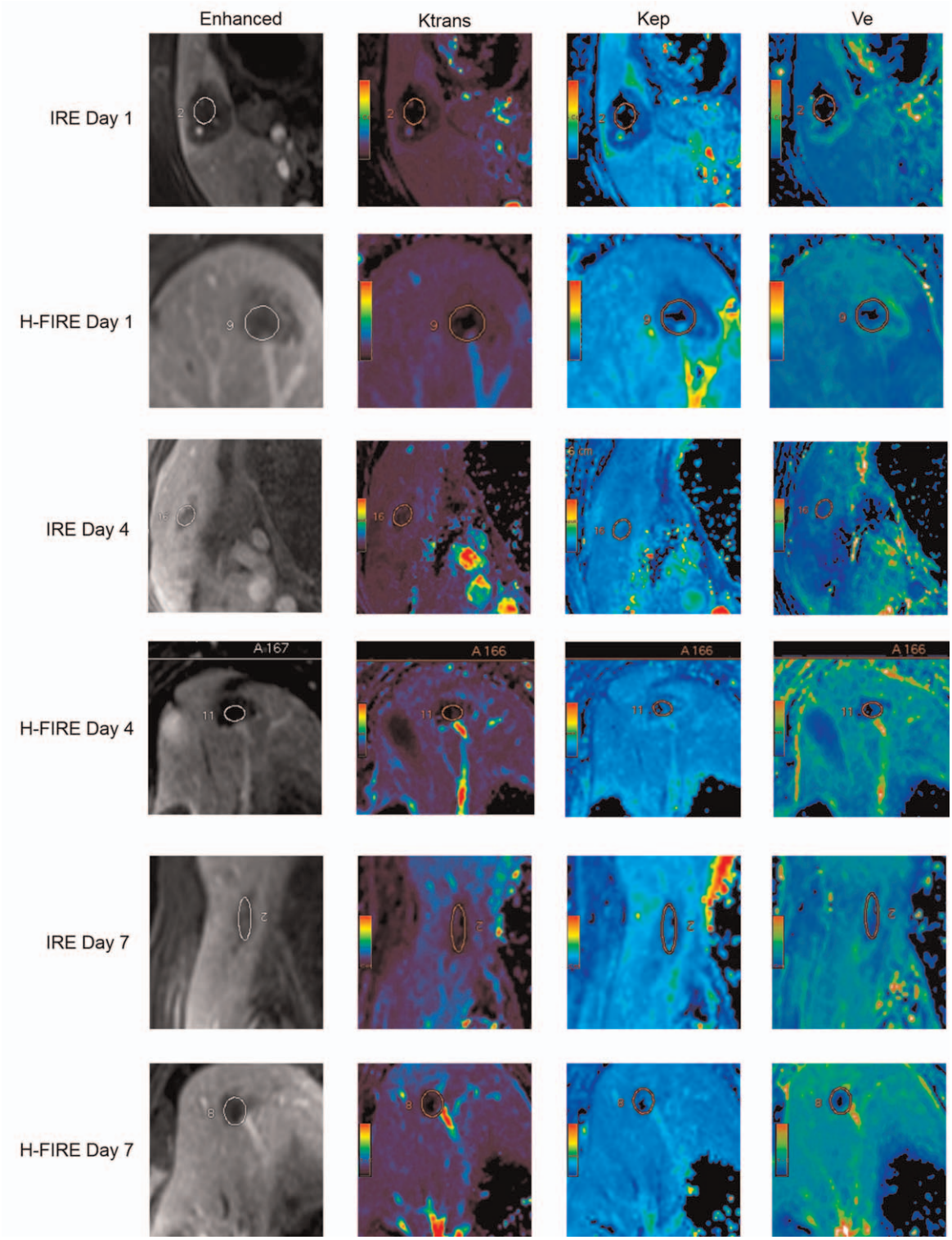

Figure 2: DCE-MRI imaging of IRE and H-FIRE lesions on day 1, day 4, and day 7 after treatment. DCE-MRI: Dynamic contrast-enhanced magnetic resonance imaging; H-FIRE: High-frequency irreversible electroporation; IRE: Irreversible electroporation; Kep: Rate constant; Ktrans: Volume transfer constant; Ve: Extravascular extracellular volume fraction. Circles represented the region of interests (ROIs).

permeability and perfusion of the tumor.[20] Previous studies found that a reduced Ktrans value in the IRE and H-FIRE zone was associated with poor perfusion and suppressed cell metabolism, indicating an enhanced ablation effect.[9,21]

Our study found no significant difference in Ktrans and Kep between IRE and H-FIRE zone, indicating similar ablation effect between the two treatments. A lower Ve value was seen in the H-FIRE zone on day 4. A significant difference in Ktrans between day 1 and day 7 was seen in

Table 2: Comparison of ablation zone sizes between IRE and H-FIRE zones on day 1, 4, and 7 (cm^2).

Time	IRE ($n = 5$)	H-FIRE ($n = 5$)	t	P
Day 1	3.20 ± 0.77	4.74 ± 0.88	3.241	0.009
Day 4	1.30 ± 0.50	2.22 ± 0.83	2.343	0.041
Day 7	0.73 ± 0.26	1.30 ± 0.68	1.928	0.083

Data are presented as mean ± standard deviation. H-FIRE: High-frequency irreversible electroporation; IRE: Irreversible electroporation.

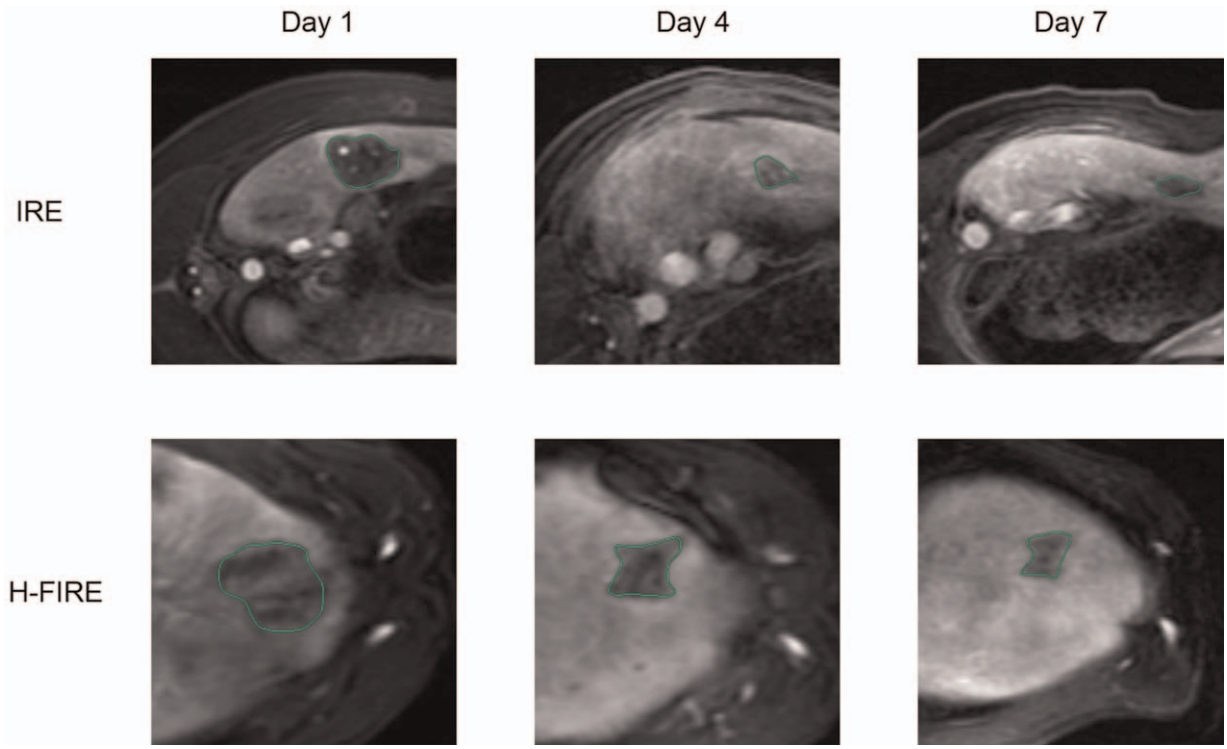

Figure 3: Sizes of ablated lesion of IRE and H-FIRE on day 1, day 4, and day 7 after treatment in DCE-MRI. Green circles represented region of interests (ROIs). DCE-MRI: Dynamic contrast-enhanced magnetic resonance imaging; H-FIRE: High-frequency irreversible electroporation; IRE: Irreversible electroporation.

the IRE zone. This impact may specifically account for the cell regeneration in H-FIRE and IRE, but not enough to reflect the difference of efficacy between the two ablation methods. The pathology analysis revealed apoptosis induced by IRE and H-FIRE, and subsequent regeneration of cell. Faroja et al[10] has reported thermal damage of IRE treatment with tissue coagulative necrosis and apoptosis. We also found slightly higher change in temperature of needle of IRE than H-FIRE, which led to similar changes on DCE-MRI of IRE and H-FIRE zone. Considering that the temperature of H-FIRE ablation area is low and the safety range is wide, the voltage or pulse times of H-FIRE can be increased to enhance the ablation effect.

The ablation zone was numerically larger in the H-FIRE zone than that in the IRE zone. The shrinking size of ablation zone over time in both IRE and H-FIRE zone indicated the cell regeneration after treatment, while the difference in ablation zone sizes between treatments gradually decreased, suggesting distinct forms of cell damage following IRE and H-FIRE treatment.

Our study found that the DCE-MRI parameters of the IRE ablation zone did not have a strong correlation with the hepatocyte counts in the ablation zone on the 7th day, which may be explained by the small number of samples and coagulative necrosis. Coagulation necrosis will decrease the metabolism in the ablation zone, making it difficult for the contrast agent to distribute. Ktrans is the rate at which the contrast agent moves from the plasma to the extravascular extracellular space, and Kep is the rate at which the contrast agent from extravascular extracellular space returns to the plasma, which reflects the local blood flow, the condition of the extracellular extravascular space and the vascular permeability together. On the 7th day after H-FIRE ablation, our study showed that the values of Kep and Ktrans in the ablation zone were correlated with the number of hepatocytes, which indicated the restoration of vascular permeability and liver cell regeneration in the ablation zone about 1 week after ablation. At this time, anticancer drugs may be given to kill the remaining tumor cells by diffusion through the blood flow into the ablation zone.

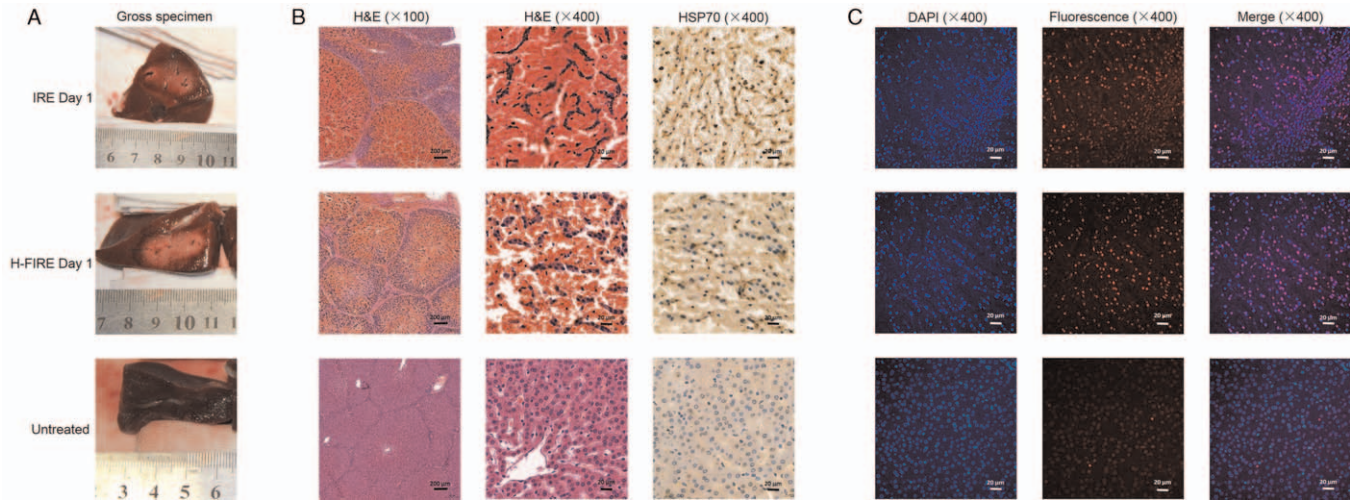

Figure 4: Histologic analysis of IRE and H-FIRE treated and untreated tissues. (A) Representative gross pathology images illustrating sections of ablation zones for 1 day after IRE (upper) and H-FIRE (middle) ablation, and the untreated liver (lower). (B) H&E staining and immunohistochemical staining of HSP70 in liver tissues after IRE (upper) and H-FIRE (middle) treatment in 1-day group, and the untreated liver (lower) (original magnification, × 100 and × 400). (C) TUNEL-stained (original magnification, × 400) representative cross-sections of liver tissues after IRE (upper) and H-FIRE (middle) treatment and untreated tissue (lower) in 1-day group. DAPI: 4', 6-diamidino-2-phenylindole; H&E: Hematoxylin-eosin; H-FIRE: High-frequency irreversible electroporation; HSP70: Heat shock protein 70; IRE: Irreversible electroporation; TUNEL: Terminal deoxynucleotidyl transferase-mediated deoxyuridine triphosphate nick-end labelling.

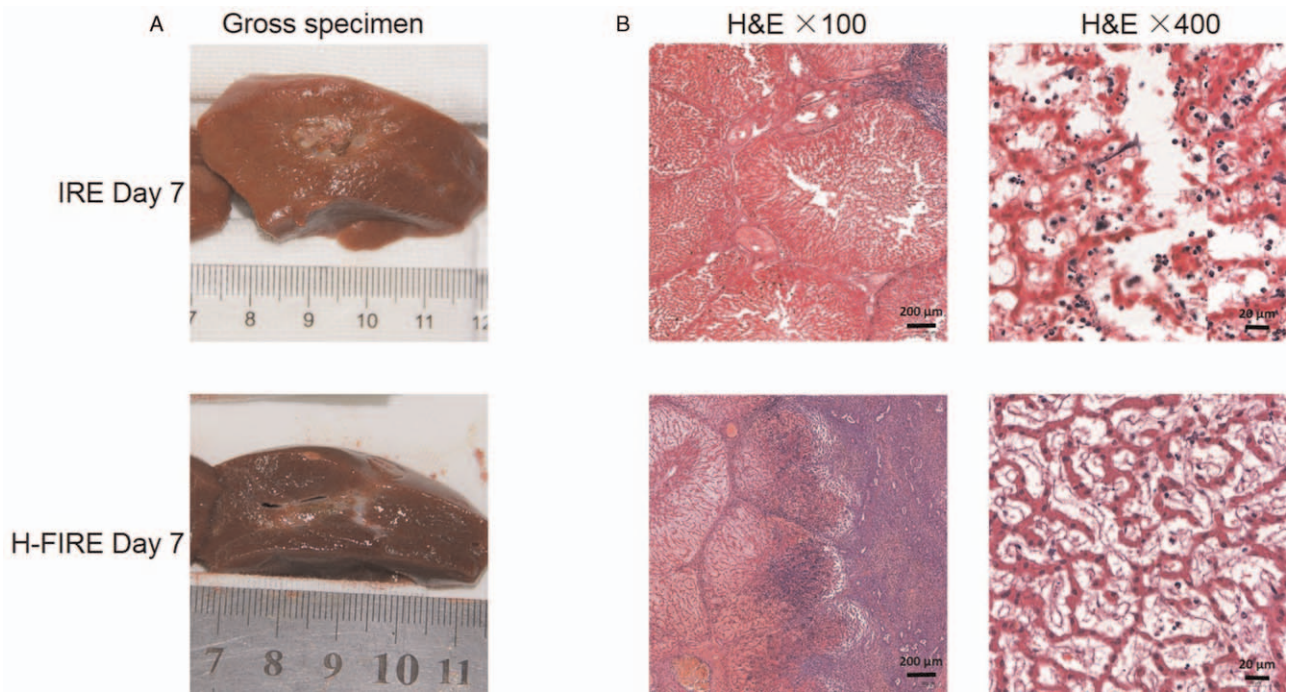

Figure 5: Representative gross pathology images illustrating sections of ablation zones 7 days after IRE (upper) and H-FIRE (lower) ablation (A). H&E staining of liver tissue after IRE (upper) and H-FIRE (lower) treatment in 7-day group (B; original magnification, × 100 and × 400). H&E staining: Hematoxylin-eosin staining; H-FIRE: High-frequency irreversible electroporation; IRE: Irreversible electroporation.

As demonstrated in the current study, nonspecific histological changes were observed directly after ablation, and cell death, featured as apoptosis and necrosis was seen after 1 day following IRE treatment. Cell death was reported to be presented as pyknosis of nuclei, karyorrhexis, and condensation of hepatocyte cytoplasm after IRE treatment.[11] Subsequently, the inflammatory response was seen approximately 6 hours after ablation. These processes progress and last 72 hours following IRE, after which the damage is replaced by fibrosis.[11] Similar results were observed in H-FIRE-treated lesions in our study. HSP70 overexpression can protect cells from stress-induced apoptosis, which is rarely seen in normal cells and frequently detected in stressed cells. Faroja et al[10] reported that coagulative necrosis and a thick rim of HSP70 were noted peripheral to the zone of ablation at high (over 60°C) temperatures, while scattered HSP70 staining was detected when the temperature was slightly

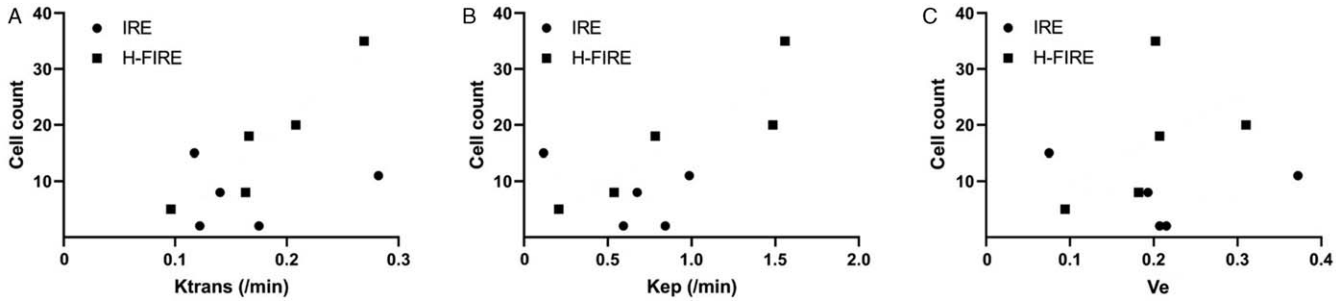

Figure 6: Correlations between the numbers of hepatic cells in the IRE ablation zone ($n = 5$) and H-FIRE ablation zone ($n = 5$) with Ktrans (A), Kep (B), and Ve (C). H-FIRE: High-frequency irreversible electroporation; IRE: Irreversible electroporation; Kep: Rate constant; Ktrans: Volume transfer constant; Ve: Extravascular extracellular volume fraction.

increased. Consistent with previous studies, the temperature was slightly increased following IRE and H-FIRE treatment, and HSP70 staining was scattered in the ablation zone. TUNEL staining indicated that the cells of ablation zone under pulsed electric field were damaged and dead. No statistical differences were detected between IRE and H-FIRE in terms of apoptotic index determined by TUNEL as well as HSP70.

Impedance in the ablation zone can change during IRE procedure,[22] requiring the monitoring of temperature during IRE. Likewise, monitoring of temperature is also necessary for H-FIRE ablation. Faroja et al[10] investigated the temperature variation of IRE, however, it should be noted that the thermistor was placed in the ablation zone instead of the needle in this study, and IRE had to be terminated when measuring temperature to avoid the interference from electric field change, which may not represent the actual temperature. In the current study, real-time measurement of temperature variation was achieved with the usage of laser through inserting a Bragg grating in the electrode to overcome the interference from electric field change. We found a low-level increase (15–20°C) of temperature in the electrode during IRE and H-FIRE treatment, as well as a slightly less temperature change following H-FIRE than IRE. With respect to safety, the MRI demonstrated that the vessels were well preserved in IRE and H-FIRE zone. Taken these findings together, H-FIRE displayed comparable safety and tolerability with IRE.

There are some limitations to our research. First of all, we cannot perform some immunohistochemical staining and cannot accurately reflect the changes of different types of cells in the ablation zone due to the lack of pig antibodies. Secondly, this study was conducted on normal liver tissues, and further study is warranted to identify the DCE-MRI characteristics after IRE and H-FIRE treatment in tumor tissues. Finally, this study was limited by the small number of samples due to the limitations of animal ethics, and larger number of samples is needed in the next step.

H-FIRE showed a comparable ablation effect to conventional IRE with a larger size of ablated lesion. A similar temperature of needle was also seen between the treatments. DCE-MRI can reflect the pathophysiological changes of H-FIRE zone.

Funding

This work was supported by a grant from the National Natural Science Foundation of China (No. 81771944).

Conflicts of interest

None.

References

1. Savic LJ, Chapiro J, Hamm B, Gebauer B, Collettini F. Irreversible electroporation in interventional oncology: where we stand and where we go. Rofo 2016;188:735–745. doi: 10.1055/s-0042-104203.
2. Davalos RV, Mir IL, Rubinsky B. Tissue ablation with irreversible electroporation. Ann Biomed Eng 2005;33:223–231. doi: 10.1007/s10439-005-8981-8.
3. Edd JF, Horowitz L, Davalos RV, Mir LM, Rubinsky B. In vivo results of a new focal tissue ablation technique: irreversible electroporation. IEEE Trans Biomed Eng 2006;53:1409–1415. doi: 10.1109/TBME.2006.873745.
4. Nielsen K, Scheffer HJ, Vieveen JM, van Tilborg AA, Meijer S, van Kuijk C, *et al*. Anaesthetic management during open and percutaneous irreversible electroporation. Br J Anaesth 2014;113:985–992. doi: 10.1093/bja/aeu256.
5. Polajžer T, Dermol-Černe J, Reberšek M, O'Connor R, Miklavčič D. Cancellation effect is present in high-frequency reversible and irreversible electroporation. Bioelectrochemistry 2020;132:107442. doi: 10.1016/j.bioelechem.2019.107442.
6. Arena CB, Sano MB, Rossmeisl JH Jr, Caldwell JL, Garcia PA, Rylander MN, *et al*. High-frequency irreversible electroporation (H-FIRE) for non-thermal ablation without muscle contraction. Biomed Eng Online 2011;10:102. doi: 10.1186/1475-925X-10-102.
7. Mercadal B, Beitel-White N, Aycock KN, Castellví Q, Davalos RV, Ivorra A. Dynamics of cell death after conventional IRE and H-FIRE treatments. Ann Biomed Eng 2020;48:1451–1462. doi: 10.1007/s10439-020-02462-8.
8. Guo Y, Zhang Y, Nijm GM, Sahakian AV, Yang GY, Omary RA, *et al*. Irreversible electroporation in the liver: contrast-enhanced inversion-recovery MR imaging approaches to differentiate reversibly electroporated penumbra from irreversibly electroporated ablation zones. Radiology 2011;258:461–468. doi: 10.1148/radiol. 10100645.
9. Shangguan AJ, Sun C, Wang B, Pan L, Ma Q, Hu S, *et al*. DWI and DCE-MRI approaches for differentiating reversibly electroporated penumbra from irreversibly electroporated ablation zones in a rabbit liver model. Am J Cancer Res 2019;9:1982–1994.
10. Faroja M, Ahmed M, Appelbaum L, Ben-David E, Moussa M, Sosna J, *et al*. Irreversible electroporation ablation: is all the damage nonthermal? Radiology 2013;266:462–470. doi: 10.1148/radiol. 12120609.
11. Vogel JA, van Veldhuisen E, Alles LK, Busch OR, Dijk F, van Gulik TM, *et al*. Time-dependent impact of irreversible electroporation on pathology and ablation size in the porcine liver: a 24-hour

experimental study. Technol Cancer Res Treat 2019;18: 1533033819876899. doi: 10.1177/1533033819876899.
12. Cong C, Qi L, Chen H. Temperature and pressure sensor based on fiber grating lasers. Beijing: Proceedings of SPIE - The International Society for Optical Engineering; 2013. doi:10. 1117/12.2031766.
13. Wasson EM, Alinezhadbalalami N, Brock RM, Allen IC, Verbridge SS, Davalos RV. Understanding the role of calcium-mediated cell death in high-frequency irreversible electroporation. Bioelectrochemistry 2020;131:107369. doi: 10.1016/j.bioelechem.2019.107369.
14. Sano MB, Fan RE, Cheng K, Saenz Y, Sonn GA, Hwang GL, *et al*. Reduction of muscle contractions during irreversible electroporation therapy using high-frequency bursts of alternating polarity pulses: a laboratory investigation in an ex vivo swine model. J Vasc Interv Radiol 2018;29:893–898.e4. doi: 10.1016/j.jvir.2017.12.019.
15. Kaufman JD, Fesmire CC, Petrella RA, Fogle CA, Xing L, Gerber D, *et al*. High-frequency irreversible electroporation using 5,000-V waveforms to create reproducible 2- and 4-cm ablation zones-a laboratory investigation using mechanically perfused liver. J Vasc Interv Radiol 2020;31:162–168.e7. doi: 10.1016/j.jvir.2019.05.009.
16. Fesmire CC, Petrella RA, Fogle CA, Gerber DA, Xing L, Sano MB. Temperature dependence of high frequency irreversible electroporation evaluated in a 3D tumor model. Ann Biomed Eng 2020; 48:2233–2246. doi: 10.1007/s10439-019-02423-w.
17. Chen BB, Shih TT. DCE-MRI in hepatocellular carcinoma-clinical and therapeutic image biomarker. World J Gastroenterol 2014; 20:3125–3134. doi: 10.3748/wjg.v20.i12.3125.
18. Tofts PS, Brix G, Buckley DL, Evelhoch JL, Henderson E, Knopp MV, *et al*. Estimating kinetic parameters from dynamic contrast-enhanced T(1)-weighted MRI of a diffusable tracer: standardized quantities and symbols. J Magn Reson Imaging 1999;10:223–232. doi: 10.1002/(sici)1522-2586(199909)10:3<223::aid-jmri2>3.0.co;2-s.
19. Yang JF, Zhao ZH, Zhang Y, Zhao L, Yang LM, Zhang MM, *et al*. Dual-input two-compartment pharmacokinetic model of dynamic contrast-enhanced magnetic resonance imaging in hepatocellular carcinoma. World J Gastroenterol 2016;22:3652–3662. doi: 10.3748/wjg.v22.i13.3652.
20. Donaldson SB, West CM, Davidson SE, Carrington BM, Hutchison G, Jones AP, *et al*. A comparison of tracer kinetic models for T1-weighted dynamic contrast-enhanced MRI: application in carcinoma of the cervix. Magn Reson Med 2010;63:691–700. doi: 10.1002/mrm.22217.
21. Tao X, Wang L, Hui Z, Liu L, Ye F, Song Y, *et al*. DCE-MRI perfusion and permeability parameters as predictors of tumor response to CCRT in Patients with locally advanced NSCLC. Sci Rep 2016;6:35569. doi: 10.1038/srep35569.
22. Lorenzo MF, Bhonsle SP, Arena CB, Davalos RV. Rapid impedance spectroscopy for monitoring tissue impedance, temperature, and treatment outcome during electroporation-based therapies. IEEE Trans Biomed Eng 2021;68:1536–1546. doi: 10.1109/TBME.2020.3036535.

How to cite this article: Li J, Zhang XB, Wang JJ, Jin LJ, Shan HS, Zhang X, Ma L, Xue XD, Zhang X, Zhang ZL, Meng LL, Yuan F, Xiao YY. Comparison between high-frequency irreversible electroporation and irreversible electroporation ablation of small swine liver: follow-up of DCE-MRI and pathological observations. Chin Med J 2021;134:2081–2090. doi: 10.1097/CM9.0000000000001663